

Boosting Universal Magnetocaloric Effect with Quantum Supercritical Scaling

Enze Lv,^{1,2} Ning Xi,¹ Yuliang Jin,^{1,2} and Wei Li^{1,2,*}

¹*Institute of Theoretical Physics, Chinese Academy of Sciences, Beijing 100190, China*

²*School of Physical Sciences, University of Chinese Academy of Sciences, Beijing 100049, China*

(Dated: October 30, 2024)

Across finite temperatures and fields, a quantum critical point (QCP) can extend to a quantum critical regime (QCR), characterized by prominent quantum fluctuations and universal scalings. The QCR is essential for comprehending many-body systems and correlated quantum materials, attracting intensive research interest over the past decades. Amongst other intriguing phenomena in QCR, the magnetocaloric effect (MCE) exhibits a universally diverging magnetic Grüneisen ratio, providing a highly sensitive indicator of the QCP. In this study, we identify a distinct quantum supercritical regime (QSR) that also originates from the QCP but is driven by a symmetry-breaking field h , which couples to the order parameter. The QSR has crossover lines following $T \propto h^{\frac{z\nu}{\beta+\gamma}}$, distinct from the renowned QCR crossovers $T \propto (g - g_c)^{z\nu}$, where β, γ, z, ν are the critical exponents. The field g controls quantum fluctuations and g_c is the critical value. Remarkably, in QSR we find the Grüneisen ratio follows $\Gamma_h \equiv \frac{1}{T}(\frac{\partial T}{\partial h})_S \propto T^{-\frac{\beta+\gamma}{z\nu}}$, which is a universal boost in MCE as compared to $\Gamma_g \equiv \frac{1}{T}(\frac{\partial T}{\partial g})_S \propto T^{-\frac{1}{z\nu}}$ in QCR. For typical $\beta + \gamma > 1$, $\Gamma_h \propto (\Gamma_g)^{\beta+\gamma}$ can lead to an increase by order of magnitude. Experimental realization involving quantum Ising and Heisenberg magnets is discussed. These systems offer an ideal platform for investigating quantum supercriticality and also hold significant potential as advanced magnetic refrigerants.

Introduction.— In quantum many-body systems with competing interactions and strong fluctuations, quantum criticality may appear by tuning external fields. Approaching a quantum critical point (QCP), the system becomes scale-invariant and highly sensitive to perturbations [1–3]. Nonclassical behaviors and universal scalings can be observed, which are independent of microscopic details but determined by the universality class associated with global constraints such as symmetry and dimensionality. Although the QCP exists at zero temperature (i.e., in the ground state), it strongly influences the thermodynamic and dynamic properties at finite temperature [1–3]. The QCP and emergent phenomena constitute a subject of extensive research in condensed matter [1, 4], ultracold atoms and ions [5], statistical and quantum field theory [6, 7], etc.

At finite temperature, a QCP expands into a quantum critical regime (QCR) that exhibits intriguing universal scalings in thermodynamic, dynamic, and transport properties, etc, stemming from the intricate interplay between quantum and thermal fluctuations [1–4, 8–10]. Among other notable phenomena, the QCR shows a universal magnetocaloric effect (MCE). Unlike traditional paramagnetic materials that reach their lowest temperatures near zero field through the adiabatic demagnetization process, the quantum critical MCE achieves its minimum temperature within the QCR. A universally diverging magnetic Grüneisen ratio $\Gamma_g \equiv \frac{1}{T}(\frac{\partial T}{\partial g})_S \propto T^{-\frac{1}{z\nu}}$ has been proposed in theory [11–16] and observed in experiments [17–23]. The universal MCE in the QCR is remarkable not only due to its nontrivial origin of emergent excitations near QCP but also because of its great ability achieving sub-Kelvin cooling [18, 24–26].

On the other hand, the symmetry-breaking field h — like the longitudinal field in the quantum Ising model (QIM) — can also be introduced near the QCP. Despite certain progresses in understanding the perturbative effects of h on low-

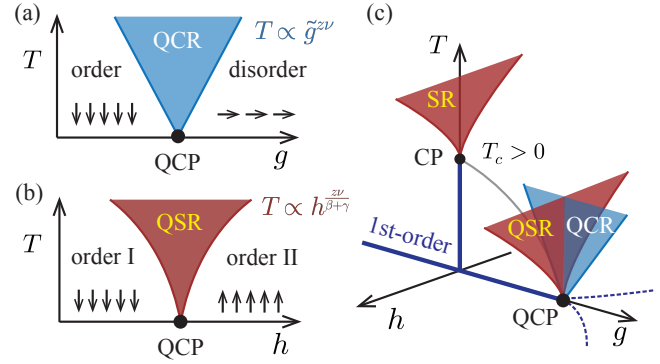


FIG. 1. (a) The QCR separates the ordered and disordered spin states in the g - T plane. Two QCR crossover lines follow the scaling $T \propto \tilde{g}^{z\nu}$, with z and ν critical exponents. The field g introduces quantum fluctuations, and $\tilde{g} \equiv g - g_c$ measures the distance to the QCP at g_c . (b) The QSR is situated between two different ordered regimes in the h - T plane, the crossover lines follow a distinct scaling $T \propto h^{\frac{z\nu}{\beta+\gamma}}$, with z, ν, β and γ being the critical exponents. (c) Above the Curie temperature T_c , there exists a classical supercritical regime (SR), which is extended down by the quantum fluctuation g and eventually becomes the QSR. The latter originates from the QCP and spans across a finite-temperature region in the h - T plane, orthogonal to the QCR situated in the g - T plane. The dashed lines $h \propto \tilde{g}^{\beta+\gamma}$ represent the quantum supercritical crossover lines proposed in Ref. [27].

energy excitations in the QIM [28–32], the impact of such symmetry-breaking fields on quantum criticality and associated scaling laws remain to be investigated. In classical statistics, the external field h couples to the order parameter and induces a first-order phase transition line between ferromagnetic (FM) states with different orientations, ending at the Curie point T_c as temperature increases [see Fig. 1(c)]. Above T_c , a classical supercritical regime emerges due to the interplay

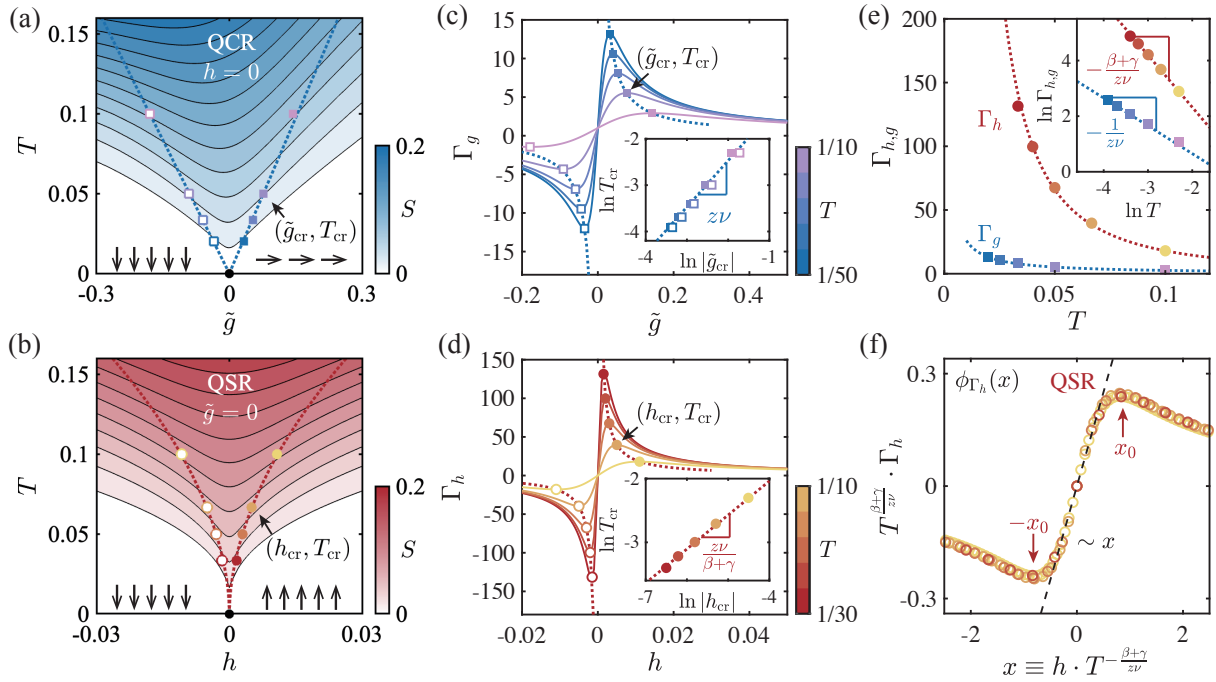


FIG. 2. The isentropes in (a) g - T plane (QCR, with $h = 0$) and (b) h - T plane (QSR, with $\tilde{g} = 0$) are illustrated, along with the corresponding Grüneisen ratio (c) Γ_g and (d) Γ_h . Circles (h_{cr}, T_{cr}) and squares (\tilde{g}_{cr}, T_{cr}), marking the peaks (dips) of Γ_g and Γ_h , compose the crossover lines, respectively. The red and blue dashed lines represent the QSR and QCR crossover lines, respectively. The insets in (c,d) highlight the distinct scaling laws: $\Gamma_g \propto T^{-\frac{1}{z\nu}}$ along the QCR crossover lines, and $\Gamma_h \propto T^{-\frac{\beta+\gamma}{z\nu}}$ along the QSR crossover lines. (e) The comparison between Γ_g and Γ_h , with the log-log plot shown in the inset, where the $\beta + \gamma$ boost is evident. (f) The scaling functions $\phi\Gamma_h(x)$ is obtained through data collapse from (d), the $\pm x_0$ points represent the crossover lines shown in (b), and QSR is in the regime $-x_0 \leq x \leq x_0$.

between thermal fluctuations and symmetry-breaking field h , highlighting the principle of universality and profound analogy between the FM and liquid-gas transitions [33]. Given that, an intriguing question arises regarding the possibility of “grafting” supercriticality onto the QCP: The quantum-fluctuation field g can suppress the Curie temperature T_c and extend it down to absolute zero [c.f., Fig. 1(c)]. Could there be a quantum supercritical regime (QSR) originating from the QCP? And would there be novel universal phenomena and effects with distinct scaling laws driven by field h ?

In this work, we unveil the existence of QSR with finite-temperature tensor network calculations on representative quantum spin models [34–37]. Figure 1(b) illustrates the QSR in the h - T plane, which is orthogonal to the QCR in the g - T plane. The QSR crossover lines and their distinct scalings are also revealed. We further discover a universal MCE characterized by diverging Grüneisen ratio with a novel, quantum supercritical scaling, $\Gamma_h \propto T^{-\frac{\beta+\gamma}{z\nu}}$, which greatly exceeds the quantum critical scaling, $\Gamma_g \propto T^{-\frac{1}{z\nu}}$, constituting a power- $(\beta + \gamma)$ boost. Furthermore, we propose to study experimentally the quantum supercritical phenomena in Ising materials [28, 38–44] and Heisenberg magnets with Dzyaloshinskii–Moriya interaction [45–54], etc, which serve as promising quantum supercritical coolants.

Models and methods.— We consider two representative models and their materialization below. One prototypical

model for revealing QSR is the FM QIM under both transverse and longitudinal fields. The QIM Hamiltonian reads $H/J = -\sum_{\langle i,j \rangle} S_i^z S_j^z - g \sum_i S_i^x - h \sum_i S_i^z$, where the coupling $J \equiv 1$ establishes the energy scale. The transverse field g drives a QCP at $g_c = 1/2$, occurring between the FM and paramagnetic phases (see Fig. 1). Instead, the longitudinal field h breaks the \mathbb{Z}_2 symmetry and induces a first-order quantum phase transition between two FM states.

We also consider the Heisenberg-Dzyaloshinskii-Moriya (HDM) model with $H/J = \sum_i \mathbf{S}_i \cdot \mathbf{S}_{i+1} + \sum_i (-1)^i D_z \hat{e}_z \cdot (\mathbf{S}_i \times \mathbf{S}_{i+1}) - B_\perp \sum_i S_i^y$, defined on a bipartite lattice, e.g., 1D chain or square lattice. Different unitary transformations can be applied to the two sublattices as D_z is alternating [46], and it results in an easy-plane XXZ model $H/J = \frac{1}{\Delta} \sum_i (S_i^x S_{i+1}^x + S_i^y S_{i+1}^y + \Delta S_i^z S_{i+1}^z) - g \sum_i S_i^y - h_s \sum_i (-1)^i S_i^x$. Here, a uniform field $g = B_\perp \cos(\frac{\alpha}{2})$ and a staggered longitudinal field $h_s = B_\perp \sin(\frac{\alpha}{2})$ are involved, where $\alpha = \text{atan } D_z$ and the anisotropy $\Delta = 1/\sqrt{1 + D_z^2}$.

Although the QSR can exist in arbitrary spatial dimensions, we focus on 1D quantum spin chains in this study without loss of generality. To simulate the finite-temperature properties, we employ the thermal tensor network approach, particularly the linearized tensor renormalization group, to compute the low-temperature properties [34–37]. In particular, we obtain the isentropic lines and magnetic Grüneisen ratio characterizing the MCE, with high accuracy and directly in the infinite-

size limit (see Fig. 5 in Appendix).

Quantum supercritical regime and universal cooling.— The QSR can be identified through calculating the thermodynamic properties and spin dynamics. From the specific heat and spin-lattice relaxation results, the QSR crossovers are revealed as $T \propto h^{\frac{z\nu}{\beta+\gamma}}$, i.e., $\propto h^{\frac{8}{15}}$ for QIM (see Appendix). Here in Fig. 2(a,b), we present the simulated isentropes of QIM, from which the QSR crossovers can also be determined and compared to those of QCR. In particular, we find the isentropic dip in the QSR is sharper than that within the QCR, and even a very small longitudinal field h can drive a dramatic temperature change.

To quantitatively compare the two cases, in Fig. 2(c,d), we show the magnetic Grüneisen ratios, i.e., Γ_g for QCR and Γ_h for QSR. Both Grüneisen ratios exhibit a peak-dip structure with a sign change as the field (g or h) crosses the QCP. In the inset of Fig. 2(d), we reveal that the peak locations $(h_{\text{cr}}, T_{\text{cr}})$ fall into scaling laws, $T_{\text{cr}} \propto h_{\text{cr}}^{\frac{z\nu}{\beta+\gamma}}$, which naturally define the QSR crossover lines in Fig. 2(b). Similarly, $T_{\text{cr}} \propto \tilde{g}_{\text{cr}}^{z\nu}$ also defines the QCR crossovers in Figs. 2(a,c). Notably, along these crossover lines the Γ_h values exceed those of Γ_g by an order of magnitude. To see that explicitly, we collect the peak values $\Gamma_h(h_{\text{cr}}, T_{\text{cr}})$ and $\Gamma_g(\tilde{g}_{\text{cr}}, T_{\text{cr}})$ and show the results in Fig. 2(e). We find Γ_h exhibits a power-law scaling $\Gamma_h \propto T^{-\frac{\beta+\gamma}{z\nu}}$, which significantly exceeds $\Gamma_g \propto T^{-\frac{1}{z\nu}}$ of QCR.

To understand this, we notice that the universally diverging Grüneisen ratio Γ_h can be expressed as $\Gamma_h = T^{-\frac{\beta+\gamma}{z\nu}} \phi_{\Gamma_h}(x)$, with $\phi_{\Gamma_h}(x)$ a scaling function and $x \equiv h T^{-\frac{\beta+\gamma}{z\nu}}$. As shown in Fig. 2(f), we obtain the scaling function $\phi_{\Gamma_h}(x)$ from an excellent collapse of the calculated data in Fig. 2(d). $\phi_{\Gamma_h}(x)$ is a parity-odd, smooth function, displaying a peak and a dip similar to Fig. 2(d), but without any singularity. The quantum supercritical behaviors observed in Fig. 2(b,d,e) can all be understood by inspecting $\phi_{\Gamma_h}(x)$. For example, as the peak/dip locates at $x = \pm x_0$ marked by the arrows in Fig. 2(f), it naturally leads to the QSR crossover lines $h = \pm x_0 \cdot T^{\frac{\beta+\gamma}{z\nu}}$ in Fig. 2(b). As the peak/dip values are finite in the universal function, one arrives at the peak/dip values $\Gamma_h = T^{-\frac{\beta+\gamma}{z\nu}} \phi_{\Gamma_h}(\pm x_0) \propto T^{-\frac{\beta+\gamma}{z\nu}}$, explaining the results in Fig. 2(e). Lastly, for small $|x| < x_0$, $\phi_{\Gamma_h}(x)$ is approximately a linear function, i.e., $\Gamma_h \cdot T^{\frac{\beta+\gamma}{z\nu}} \propto x$ [see Fig. 2(f)]. Recalling that $x \equiv h \cdot T^{-\frac{\beta+\gamma}{z\nu}}$, we find that $\Gamma_h/h \propto T^{-2\frac{\beta+\gamma}{z\nu}}$, demonstrating a very strong divergence for each fixed h and within the QSR (see Fig. 7 of the Appendix). This scaling law, together with the $\Gamma_h \propto T^{-\frac{\beta+\gamma}{z\nu}}$ scaling on QSR crossover lines, characterize the boosted quantum supercritical MCE.

Universal hyperscaling function and crossover surface.— More generally, near a QCP the Grüneisen ratio Γ_h can be described as a two-variable hyperscaling function, $\Gamma_h = T^{-\frac{\beta+\gamma}{z\nu}} \psi_{\Gamma_h}(x, y)$, with x defined above and $y \equiv \tilde{g} \cdot T^{-\frac{1}{z\nu}}$. In Fig. 3(a), we show the obtained function $\psi_{\Gamma_h}(x, y)$ through data collapsing. The red solid lines mark the peaks and dips of $\psi_{\Gamma_h}(x, y)$ by scanning x for each fixed y , and each point (x_i, y_i) represents a crossover line in Fig. 3(b). For example,

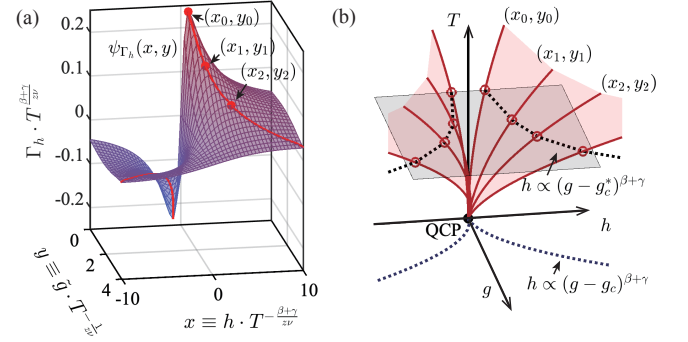


FIG. 3. (a) The hyperscaling function $\psi_{\Gamma_h}(x, y)$ obtained through data collapsing. The red lines indicate the locations of peaks/dips in $\psi_{\Gamma_h}(x, y)$ landscape when scanning x for various fixed y . Each point (x_i, y_i) in (a) corresponds to a crossover line in (b), where the lines form a crossover surface in the g - h - T diagram. The gray plane represents an isothermal cut, where the dashed intersection lines connect the locations of maxima in Γ_h at finite T . In the low temperature limit, the intersection line follows $h \propto (g - g_c)^{\beta+\gamma}$, i.e., quantum supercritical crossovers in the g - h plane proposed in Ref. [27].

the point with $(x_0, y_0 = 0)$ corresponds to the crossover line for the case $g = g_c$ [see also in Fig. 2(b)]. As (x_i, y_i) moves, the crossover lines form a crossover surface in Fig. 3(b), enclosing a generalized QSR for $\tilde{g} \neq 0$. Notably, an isothermal plane at a fixed temperature T (gray plane) intersects the crossover surfaces, resulting in two dashed lines that follow the scaling $h \propto (g - g_c^*)^{\beta+\gamma}$ (with g_c^* the pseudo-QCP estimated at finite temperature, see Fig. 8 in Appendix). In the zero-temperature limit, $g_c^* = g_c$, and the dashed line in Fig. 1(c) is nothing but the supercritical crossover line $h \propto \tilde{g}^{\beta+\gamma}$ in the g - h quantum phase diagram [27].

Quantum supercritical coolant.— Quantum magnets provide an ideal platform to investigate exotic quantum many-body phenomena and effects. Here we propose to observe the quantum supercritical MCE in two kinds of magnets: the Ising-chain and HDM compounds. The spin-chain material CoNb_2O_6 has FM Ising interaction $J \simeq 28.8$ K, and a QCP exists at $B_x^c = 5.25$ T [28, 38–41]. Although some additional interactions may also exist [41, 56], the 1+1D Ising universality class remains. Therefore, we use the QIM to analyze the universal scalings in CoNb_2O_6 near the QCP. In Fig. 4(a), we show that a significant temperature change can be induced by a small longitudinal field B_z . Starting from 1.8 K and 1.3 K, the system cools down to 280 mK and 52 mK, respectively, as B_z changes from 0.15 T to zero. These results, based on realistic material parameters, demonstrate that even a modest longitudinal field can induce dramatic temperature variations near the QCP.

The second example showing pronounced supercritical MCE is HDM material. Under an in-plane field B_{\perp} (i.e., perpendicular to the D_z axis), the HDM system can be effectively represented as an easy-plane Heisenberg model with $\Delta < 1$, subjected to a uniform field g and a staggered field h_s , both within the easy plane [see inset in Fig. 4(b)]. The

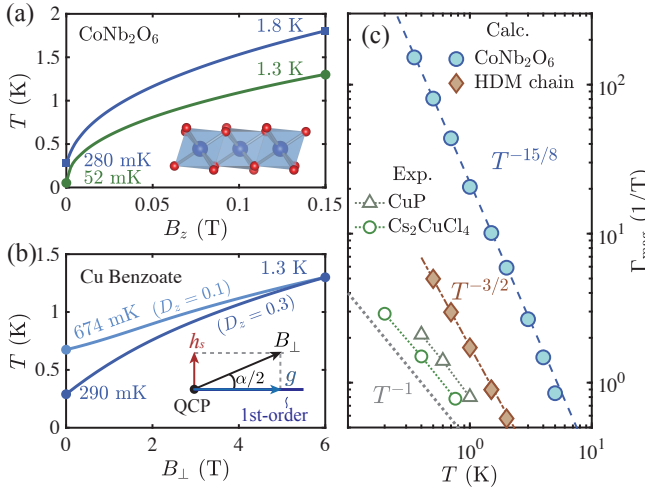


FIG. 4. (a) Simulated isentropic lines of CoNb_2O_6 by varying the longitudinal field B_z , while the transverse field is fixed at $B_x^c \approx 5.25$ T. Inset shows the lattice structure of CoNb_2O_6 . (b) Simulated isentropic line of the representative HDM compounds Cu benzoate ($J \approx 18.2$ K, $D_z \approx 0.1$) under a in-plane field B_\perp . The dark blue line represents the isentropic line for $D_z = 0.3$. Inset illustrates the effective transverse field g and staggered longitudinal field h_s associated with an external magnetic field B_\perp . (c) Temperature scalings of Grüneisen peak value for various materials. Blue circles and brown diamonds represent the calculated results of CoNb_2O_6 and HDM systems ($D_z = 0.3$ and $\Gamma_{h_s} \equiv \frac{1}{T}(\frac{\partial T}{\partial h_s})_S$ is shown), respectively. The hollow dots are from experimental results of different materials, such as the triangular-lattice Heisenberg antiferromagnet Cs_2CuCl_4 [19] and spin chain CuP [55].

uniform field g controls the quantum fluctuations and drives a Berezinskii-Kosterlitz-Thouless quantum phase transition at zero field; while the staggered field h_s breaks the \mathbb{Z}_2 symmetry and gives rise to quantum supercritical phenomena [57]. In this case, when comparing quantum critical cooling induced by g with supercritical cooling driven by h_s , the latter significantly outperforms the former (see Appendix).

The HDM compounds, including Cu benzoate [45–50], Cu-PM [51], Yb_4As_3 [52, 53] and KCuGaF_6 [54], etc, have been studied for decades. The DM coupling parameters D_z ranges from 0.1 to about 0.3 in these compounds. Here, we consider a representative HDM chain, Cu benzoate with $D_z \approx 0.1$, and artificially increase its value to $D_z = 0.3$ to investigate the supercritical MCE. Starting from the initial condition $T = 1.3$ K and $B = 6$ T (thus $h_s \approx 0.8$ T for $D_z = 0.3$), the system with $D_z = 0.3$ reaches the lowest temperature of 290 mK near zero field [see Fig. 4(b)]. The results reveal that beyond the prototypical Ising system, Heisenberg compound with additional couplings, like the D_z term, can also exhibit prominent quantum supercritical MCE.

To compare the quantum critical and supercritical cooling, we collect the peak values in the Grüneisen ratios by scanning the field at each fixed temperature [c.f., Fig. 2(c,d)]. In Fig. 4(c), we see that the compound CoNb_2O_6 demonstrates a supercritical scaling $\Gamma_B \propto T^{-\frac{\beta+\gamma}{z\nu}} = T^{-15/8}$,

significantly exceeding other compounds with QCR, where $\Gamma_B \propto T^{-\frac{1}{z\nu}} = T^{-1}$ [19, 22, 55]. In addition, we also show the simulated Grüneisen peaks of the HDM chain in Fig. 4(c), where a $T^{-3/2}$ scaling is observed [57]. It surpasses the $1/T$ scaling of quantum critical coolants, e.g., the pure Heisenberg chain CuP, shown in the same figure.

Discussion and outlook.— As the endpoint of a first-order transition line [c.f., Fig. 1(c)], universal scaling behaviors emerge in the supercritical regime [33]. Among other phenomena, there exists prominent MCE near the Curie point, which can be traced back to the seminal work of Weiss and Piccard in 1917 — the first observation of “very sensitive temperature variations in relation to the magnetic field” in nickel [58, 59]. From a modern perspective, given that temperature variations are most pronounced above the Curie point, such MCE can be considered as a supercritical phenomenon. Below the Curie point, the spontaneous magnetization contributes only a minor effect [58], and the MCE quickly diminishes. Consequently, T_c sets a critical limitation for magnetic refrigerants, hindering their ability to reach lower temperatures. Historically, hydrated paramagnetic salts with dilute magnetic ions and thus low T_c are used to first achieve sub-Kelvin refrigeration [60]. However, this approach also has significant drawbacks: the cooling capacity and thermal conductivity are severely limited due to the very low density of magnetic ions, reduced by about one order of magnitude.

In this study, we turn to quantum fluctuations that can effectively suppress T_c down to absolute zero without reducing ion density. The classical supercritical regime becomes a QSR above QCP, exhibiting universal MCE as characterized by the longitudinal-field Grüneisen ratio Γ_h . It diverges with quantum supercritical scaling as T lowers, extending all the way to zero temperature without any finite-temperature constraints.

Although both originating from the QCP, the proposed QSR here is intrinsically different from the well-studied QCR, existing in an h - T plane orthogonal to the g - T plane of the latter. The two have crossover lines of distinct scalings, i.e., $T \propto h^{\frac{z\nu}{\beta+\gamma}}$ vs. $T \propto \tilde{g}^{z\nu}$. The fundamental difference between QSR and QCR results in diverse universal phenomena, properties, and effects. By comparing the universal MCE between the two, we find the Grüneisen ratio diverges much faster in QSR than that in QCR, amplified by a power of $(\beta + \gamma)$. In the simulations with material parameters, we find such distinct scalings can lead to an enhancement in Grüneisen ratio values by orders of magnitude.

Moreover, such boosted quantum supercritical cooling can be explored in experiments. For the HDM magnets, like Cu benzoate [45–47] or Yb_4As_3 [52, 53], we suggest that a prominent cooling effect can be observed through an adiabatic demagnetization process. For the Ising magnet CoNb_2O_6 , on the other hand, we propose to investigate its QSR by slightly tilting the magnetic fields. A small longitudinal field is introduced in tilted fields, while keeping the transverse component largely unchanged. For instance, by adjusting the field angle by approximately 2°, the longitudinal field reaches $h \approx 0.2$ T, and a transverse field of $g \approx 5.25$ T remains in close prox-

imity to the QCP in CoNb_2O_6 , making it suitable to generate a strong quantum supercritical cooling effect. This field-tilting technique has been demonstrated in the studies of 3D Ising magnets such as LiREF_4 [42, 43], and consequently, we believe that our proposal for universal quantum supercritical cooling is not only feasible but also readily accessible given existing methodologies.

Lastly, quantum supercriticality is not limited in quantum magnets but also pertinent for other field-tunable quantum materials, e.g., the strongly correlated metal near the pressure-induced FM QCP [61]. Besides universal MCE discussed above, we emphasize the aspects of spin dynamics, transport properties, and even non-equilibrium physics in the QSR remains to be explored. Overall, our work lays down the foundation and open up new avenues for investigating the intriguing quantum supercritical phenomena and effects, using quantum magnets in specific and correlated materials in general.

Acknowledgments.— E.L. and W.L. are indebted to Junsen Wang, Xinyang Li, and Yang Qi for stimulating discussions. This work was supported by the National Natural Science Foundation of China (Grant Nos. 12222412 and 12047503), and the CAS Project for Young Scientists in Basic Research (YSBR-057). We thank the HPC-ITP for the technical support and generous allocation of CPU time.

* w.li@itp.ac.cn

[1] S. Sachdev, Quantum criticality: Competing ground states in low dimensions, *Science* **288**, 475 (2000).

[2] P. Coleman and A. J. Schofield, Quantum criticality, *Nature* **433**, 226 (2005).

[3] S. Sachdev, *Quantum phase transitions*, 2nd ed. (Cambridge University Press, Cambridge, 2015).

[4] S. L. Sondhi, S. M. Girvin, J. P. Carini, and D. Shahar, Continuous quantum phase transitions, *Rev. Mod. Phys.* **69**, 315 (1997).

[5] X. Zhang, C.-L. Hung, S.-K. Tung, and C. Chin, Observation of quantum criticality with ultracold atoms in optical lattices, *Science* **335**, 1070 (2012).

[6] S. Sachdev and M. Müller, Quantum criticality and black holes, *J. Phys.: Condens. Matter* **21**, 164216 (2009).

[7] M. Čubrović, J. Zaanen, and K. Schalm, String theory, quantum phase transitions, and the emergent Fermi liquid, *Science* **325**, 439 (2009).

[8] S. Sachdev and J. Ye, Universal quantum-critical dynamics of two-dimensional antiferromagnets, *Phys. Rev. Lett.* **69**, 2411 (1992).

[9] S. Kirchner, S. Paschen, Q. Chen, S. Wirth, D. Feng, J. D. Thompson, and Q. Si, Colloquium: Heavy-electron quantum criticality and single-particle spectroscopy, *Rev. Mod. Phys.* **92**, 011002 (2020).

[10] M. Continentino, *Quantum scaling in many-body systems*, 2nd ed. (Cambridge University Press, Cambridge, 2017).

[11] L. Zhu, M. Garst, A. Rosch, and Q. Si, Universally diverging Grüneisen parameter and the magnetocaloric effect close to quantum critical points, *Phys. Rev. Lett.* **91**, 066404 (2003).

[12] M. E. Zhitomirsky and A. Honecker, Magnetocaloric effect in one-dimensional antiferromagnets, *J. Stat. Mech.: Theor. Exp.* **2004**, 07012 (2004).

[13] M. Garst and A. Rosch, Sign change of the Grüneisen parameter and magnetocaloric effect near quantum critical points, *Phys. Rev. B* **72**, 205129 (2005).

[14] J. Wu, L. Zhu, and Q. Si, Entropy accumulation near quantum critical points: effects beyond hyperscaling, *J. Phys.: Conf. Ser.* **273**, 012019 (2011).

[15] A. Honecker and S. Wessel, Magnetocaloric effect in quantum spin- s chains, *Condens. Matter Phys.* **12**, 399 (2009).

[16] L. Zhang, Universal thermodynamic signature of self-dual quantum critical points, *Phys. Rev. Lett.* **123**, 230601 (2019).

[17] B. Wolf, Y. Tsui, D. Jaiswal-Nagar, U. Tutsch, A. Honecker, K. Remović-Langer, G. Hofmann, A. Prokofiev, W. Assmus, G. Donath, and M. Lang, Magnetocaloric effect and magnetic cooling near a field-induced quantum-critical point, *Proc. Natl. Acad. Sci. U.S.A.* **108**, 6862 (2011).

[18] M. Lang, B. Wolf, A. Honecker, Y. Tsui, D. Jaiswal-Nagar, U. Tutsch, G. Hofmann, A. Prokofiev, P. T. Cong, N. Krüger, F. Ritter, and W. Assmus, Magnetic cooling through quantum criticality, *J. Phys.: Conf. Series* **400**, 032043 (2012).

[19] B. Wolf, A. Honecker, W. Hofstetter, U. Tutsch, and M. Lang, Cooling through quantum criticality and many-body effects in condensed matter and cold gases, *Int. J. Mod. Phys. B* **28**, 1430017 (2014).

[20] Y. Tokiwa, T. Radu, C. Geibel, F. Steglich, and P. Gegenwart, Divergence of the magnetic Grüneisen ratio at the field-induced quantum critical point in YbRh_2Si_2 , *Phys. Rev. Lett.* **102**, 066401 (2009).

[21] Y. Tokiwa, C. Stingl, M.-S. Kim, T. Takabatake, and P. Gegenwart, Characteristic signatures of quantum criticality driven by geometrical frustration, *Sci. Adv.* **1**, e1500001 (2015).

[22] P. Gegenwart, Grüneisen parameter studies on heavy fermion quantum criticality, *Rep. Prog. Phys.* **79**, 114502 (2016).

[23] B. Wolf, U. Tutsch, S. Dörschug, C. Krellner, F. Ritter, W. Assmus, and M. Lang, Magnetic cooling close to a quantum phase transition—the case of $\text{Er}_2\text{Ti}_2\text{O}_7$, *J. Appl. Phys.* **120**, 142112 (2016).

[24] M. E. Zhitomirsky, Enhanced magnetocaloric effect in frustrated magnets, *Phys. Rev. B* **67**, 104421 (2003).

[25] X.-Y. Liu, Y. Gao, H. Li, W. Jin, J. Xiang, H. Jin, Z. Chen, W. Li, and G. Su, Quantum spin liquid candidate as superior refrigerant in cascade demagnetization cooling, *Commun. Phys.* **5**, 233 (2022).

[26] J. Xiang, C. Zhang, Y. Gao, W. Schmidt, K. Schmalzl, C.-W. Wang, B. Li, N. Xi, X.-Y. Liu, H. Jin, G. Li, J. Shen, Z. Chen, Y. Qi, Y. Wan, W. Jin, W. Li, P. Sun, and G. Su, Giant magnetocaloric effect in spin supersolid candidate $\text{Na}_2\text{BaCo}(\text{PO}_4)_2$, *Nature* **625**, 270 (2024).

[27] J. Wang, E. Lv, X. Li, Y. Jin, and W. Li, Quantum supercriticality in the Ising model and Rydberg atom array, *arXiv:2407.05455*.

[28] R. Coldea, D. A. Tennant, E. M. Wheeler, E. Wawrzynska, D. Prabhakaran, M. Telling, K. Habicht, P. Smeibidl, and K. Kiefer, Quantum criticality in an Ising chain: Experimental evidence for emergent E_8 symmetry, *Science* **327**, 177 (2010).

[29] C. M. Morris, R. Valdés Aguilar, A. Ghosh, S. M. Koohpayeh, J. Krizan, R. J. Cava, O. Tchernyshyov, T. M. McQueen, and N. P. Armitage, Hierarchy of bound states in the one-dimensional ferromagnetic Ising chain CoNb_2O_6 investigated by high-resolution time-domain terahertz spectroscopy, *Phys. Rev. Lett.* **112**, 137403 (2014).

[30] Y. Cui, H. Zou, N. Xi, Z. He, Y. X. Yang, L. Shu, G. H. Zhang, Z. Hu, T. Chen, R. Yu, J. Wu, and W. Yu, Quantum criticality of the Ising-like screw chain antiferromagnet $\text{SrCo}_2\text{V}_2\text{O}_8$ in a transverse magnetic field, *Phys. Rev. Lett.* **123**, 067203 (2019).

[31] Z. Zhang, K. Amelin, X. Wang, H. Zou, J. Yang, U. Nagel, T. Rö om, T. Dey, A. A. Nugroho, T. Lorenz, J. Wu, and Z. Wang, Observation of E_8 particles in an Ising chain antiferromagnet, *Phys. Rev. B* **101**, 220411 (2020).

[32] H. Zou, Y. Cui, X. Wang, Z. Zhang, J. Yang, G. Xu, A. Okutani, M. Hagiwara, M. Matsuda, G. Wang, G. Mussardo, K. Hódsági, M. Kormos, Z. He, S. Kimura, R. Yu, W. Yu, J. Ma, and J. Wu, E_8 spectra of quasi-one-dimensional antiferromagnet $\text{BaCo}_2\text{V}_2\text{O}_8$ under transverse field, *Phys. Rev. Lett.* **127**, 077201 (2021).

[33] X. Li and Y. Jin, Thermodynamic crossovers in supercritical fluids, *Proc. Natl. Acad. Sci.* **121** (2024).

[34] W. Li, S.-J. Ran, S.-S. Gong, Y. Zhao, B. Xi, F. Ye, and G. Su, Linearized tensor renormalization group algorithm for the calculation of thermodynamic properties of quantum lattice models, *Phys. Rev. Lett.* **106**, 127202 (2011).

[35] Y.-L. Dong, L. Chen, Y.-J. Liu, and W. Li, Bilayer linearized tensor renormalization group approach for thermal tensor networks, *Phys. Rev. B* **95**, 144428 (2017).

[36] B.-B. Chen, L. Chen, Z. Chen, W. Li, and A. Weichselbaum, Exponential thermal tensor network approach for quantum lattice models, *Phys. Rev. X* **8**, 031082 (2018).

[37] Q. Li, Y. Gao, Y.-Y. He, Y. Qi, B.-B. Chen, and W. Li, Tangent space approach for thermal tensor network simulations of the 2D Hubbard model, *Phys. Rev. Lett.* **130**, 226502 (2023).

[38] T. Liang, S. M. Kooohpayeh, J. W. Krizan, T. M. McQueen, R. J. Cava, and N. P. Ong, Heat capacity peak at the quantum critical point of the transverse Ising magnet CoNb_2O_6 , *Nat. Comm.* **6**, 7611 (2015).

[39] C. M. Morris, N. Desai, J. Viirok, D. Huvonen, U. Nagel, T. Rö öm, J. W. Krizan, R. J. Cava, T. M. McQueen, S. M. Kooohpayeh, R. K. Kaul, and N. P. Armitage, Duality and domain wall dynamics in a twisted Kitaev chain, *Nat. Phys.* **17**, 832 (2021).

[40] Y. Xu, L. S. Wang, Y. Y. Huang, J. M. Ni, C. C. Zhao, Y. F. Dai, B. Y. Pan, X. C. Hong, P. Chauhan, S. M. Kooohpayeh, N. P. Armitage, and S. Y. Li, Quantum critical magnetic excitations in spin-1/2 and spin-1 chain systems, *Phys. Rev. X* **12**, 021020 (2022).

[41] L. Woodland, D. Macdougal, I. M. Cabrera, J. D. Thompson, D. Prabhakaran, R. I. Bewley, and R. Coldea, Tuning the confinement potential between spinons in the Ising chain CoNb_2O_6 using longitudinal fields and quantitative determination of the microscopic Hamiltonian, *Phys. Rev. B* **108**, 184416 (2023).

[42] A. Wendl, H. Eisenlohr, F. Rucker, C. Duvinage, M. Kleinhans, M. Vojta, and C. Pfleiderer, Emergence of mesoscale quantum phase transitions in a ferromagnet, *Nature* **609**, 65 (2022).

[43] P. Liu, D. Yuan, C. Dong, G. Lin, E. G. Víllora, J. Qi, X. Zhao, K. Shimamura, J. Ma, J. Wang, Z. Zhang, and B. Li, Ultralow-field magnetocaloric materials for compact magnetic refrigeration, *NPG Asia Materials* **15**, 41 (2023).

[44] H. Xie, L. Tian, Q. Chen, H. Sun, X. Gao, Z. Li, Z. Mo, and J. Shen, Giant and reversible low field magnetocaloric effect in LiHoF_4 compound, *Dalton Trans.* **50**, 17697 (2021).

[45] F. H. L. Essler and A. M. Tsvelik, Dynamical magnetic susceptibilities in copper benzoate, *Phys. Rev. B* **57**, 10592 (1998).

[46] M. Oshikawa and I. Affleck, Field-induced gap in $S = 1/2$ antiferromagnetic chains, *Phys. Rev. Lett.* **79**, 2883 (1997).

[47] I. Affleck and M. Oshikawa, Field-induced gap in Cu benzoate and other $S = \frac{1}{2}$ antiferromagnetic chains, *Phys. Rev. B* **60**, 1038 (1999).

[48] J. Lou, S. Qin, C. Chen, Z. Su, and L. Yu, Field-induced gap in the spin- $\frac{1}{2}$ antiferromagnetic Heisenberg chain: A density-matrix renormalization-group study, *Phys. Rev. B* **65**, 064420 (2002).

[49] J. Z. Zhao, X. Q. Wang, T. Xiang, Z. B. Su, and L. Yu, Effects of the Dzyaloshinskii-Moriya interaction on low-energy magnetic excitations in copper benzoate, *Phys. Rev. Lett.* **90**, 207204 (2003).

[50] J. Lou, C. Chen, J. Zhao, X. Wang, T. Xiang, Z. Su, and L. Yu, Midgap states in antiferromagnetic Heisenberg chains with a staggered field, *Phys. Rev. Lett.* **94**, 217207 (2005).

[51] S. A. Zvyagin, A. K. Kolezhuk, J. Krzystek, and R. Feyerherm, Excitation hierarchy of the quantum sine-Gordon spin chain in a strong magnetic field, *Phys. Rev. Lett.* **93**, 027201 (2004).

[52] M. Oshikawa, K. Ueda, H. Aoki, A. Ochiai, and M. Kohgi, Field-induced gap formation in Yb_4As_3 , *Journal of the Physical Society of Japan* **68**, 3181 (1999).

[53] M. Kohgi, K. Iwasa, J.-M. Mignot, B. Fåk, P. Gegenwart, M. Lang, A. Ochiai, H. Aoki, and T. Suzuki, Staggered field effect on the one-dimensional $S = \frac{1}{2}$ antiferromagnet Yb_4As_3 , *Phys. Rev. Lett.* **86**, 2439 (2001).

[54] I. Umegaki, H. Tanaka, N. Kurita, T. Ono, M. Laver, C. Niedermayer, C. Rüegg, S. Ohira-Kawamura, K. Nakajima, and K. Kakurai, Spinon, soliton, and breather in the spin- $\frac{1}{2}$ antiferromagnetic chain compound KCuGaF_6 , *Phys. Rev. B* **92**, 174412 (2015).

[55] O. Breunig, M. Garst, A. Klümper, J. Rohrkamp, M. M. Turnbull, and T. Lorenz, Quantum criticality in the spin-1/2 Heisenberg chain system copper pyrazine dinitrate, *Sci. Adv.* **3**, eaao3773 (2017).

[56] M. Fava, R. Coldea, and S. A. Parameswaran, Glide symmetry breaking and Ising criticality in the quasi-1D magnet CoNb_2O_6 , *Proc. Natl. Acad. Sci.* **117**, 25219 (2020).

[57] According to the quantum scaling analysis of easy-plane Heisenberg chain, the crossover line driven by the staggered field follows a $T \propto h_s^{1/(2-d)}$ scaling [46, 62], where $1/4 < d < 1/2$ is the scaling dimension. The Grüneisen ratio thus follows $\Gamma_B \propto T^{\tilde{d}=d-2}$ with $-3/2 < \tilde{d} < -7/4$.

[58] P. Weiss and A. Piccard, Le phénomène magnétocalorique, *J. Phys. (Paris)* **7**, 103 (1917).

[59] Smith, Anders, Who discovered the magnetocaloric effect? - Warburg, Weiss, and the connection between magnetism and heat, *Eur. Phys. J. H* **38**, 507 (2013).

[60] W. F. Giauque and D. P. MacDougall, Attainment of temperatures below 1° absolute by demagnetization of $\text{Gd}_2(\text{SO}_4)_3 \cdot 8\text{H}_2\text{O}$, *Phys. Rev.* **43**, 768 (1933).

[61] S. Bin, Z. Yongjun, K. Yashar, N. Michael, B. Robert, W. An, C. Ye, N. Zhiyong, L. Rui, L. Xin, L. Hanoh, S. Michael, S. Frank, P. Coleman, and H. Yuan, Strange-metal behaviour in a pure ferromagnetic Kondo lattice, *Nature* **579**, 51 (2020).

[62] E. Fradkin, *Field theories of condensed matter physics* (Cambridge University Press, 2013).

[63] N. Xi, Y. Gao, C. Li, S. Liang, R. Yu, X. Wang, and W. Li, Thermal tensor network approach for spin-lattice relaxation in quantum magnets, *arXiv:2403.11895*.

End Matter

Linearized tensor renormalization group.— The linearized tensor renormalization group (LTRG) method [34, 35] can be employed to accurately compute the low-temperature properties of infinite-size systems. Taking the 1D system as an example, we decompose the Hamiltonian as H_{ab} and H_{ba} for even and odd bonds, respectively [see Fig. 5(a)]. Through the Trotter-Suzuki decomposition, the density matrix can be expressed as $\rho(\beta) = e^{-\beta H} \approx (e^{-\tau H_{ab}} e^{-\tau H_{ba}})^n$, where $\tau = \beta/n$ is the Trotter step and $\beta = 1/T$ is the inverse temperature. In practice, the partition function, $Z(\beta) = \text{Tr}[\rho(\beta/2)\rho(\beta/2)^\dagger]$, can be calculated by contracting the thermal tensor network. For the quantum Ising and Heisenberg models considered in the main text, the calculated results are well converged and highly accurate by retaining up to 600 bond states. As shown in Fig. 5(b), the relative error of specific heat is less than 10^{-3} even down to $T/J = 0.01$.

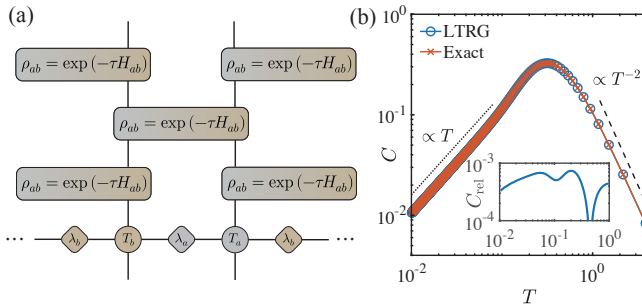


FIG. 5. (a) The finite-temperature density operator can be obtained via imaginary-time evolution. The density operator consists of local tensors λ_a , T_a , λ_b , and T_b , and the evolution gates are $\rho_{ab}(\tau) = \exp(-\tau H_{ab})$ and $\rho_{ba}(\tau) = \exp(-\tau H_{ba})$. (b) The calculated specific heat C_{sim} of the QIM at the critical field $g = g_c$ (blue circles), which lie on the bottom of the exact solution C_{exact} (red crosses). The dotted line illustrates the power-law scaling $C \propto T$ in the low and the dashed line shows high-temperature behavior $C \propto T^{-2}$. Inset shows the relative error $C_{\text{rel}} \equiv |C_{\text{exact}} - C_{\text{sim}}|/C_{\text{exact}} \lesssim 10^{-3}$.

Scalings of thermodynamics and spin dynamics in QSR.— In Fig. 6(a,b), we present the contours of specific heat C/T of the FM quantum Ising chain. The QCR crossover lines, $T \propto \tilde{g}^{z\nu}$, are straight for the 1+1D Ising universality class. Distinctly, the QSR crossover lines are curved, following $T \propto h^{\frac{z\nu}{\beta+\gamma}}$ (i.e., $\propto h^{\frac{8}{15}}$). As shown in Fig. 6(c), the specific heat follows $C \propto T^{\frac{d}{z}}$ (i.e., $\propto T$) within the QSR, and deviates such universal scaling at sufficiently low temperatures. The peak locations of C/T can be used to determine the QSR crossover lines in the h - T plane, as shown in the inset of Fig. 6(c).

It is fascinating to explore whether universal quantum supercritical scalings also manifest itself in finite-temperature spin dynamics. We consider the spin-lattice relaxation rate in nuclear magnetic resonance measurements, i.e., $1/T_1 \propto \mathcal{S}_1(\omega = 0) \simeq \lim_{\omega \rightarrow 0} T \sum_{\alpha=x,y,z} \chi''_{\alpha\alpha}(\omega)/\omega$, where $\chi''_{\alpha\alpha}(\omega)$ is the local dynamical susceptibility. With thermal tensor

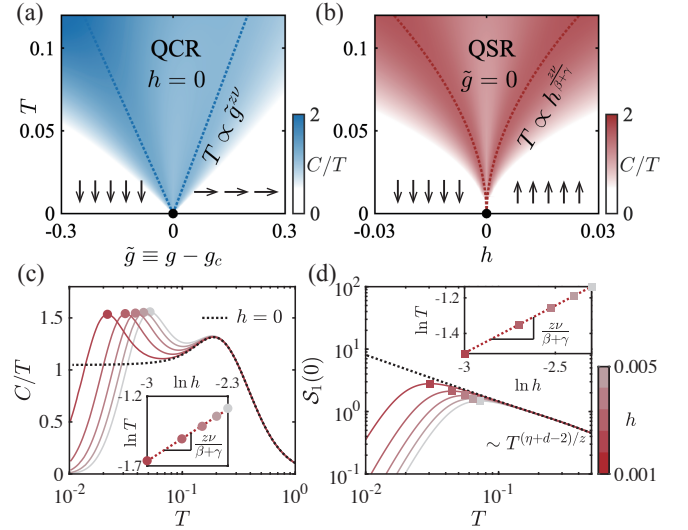


FIG. 6. (a,b) Contour plots of C/T are presented. The dashed lines tracing the peaks of C/T vs. T , represent the crossover lines of QCR ($T \propto \tilde{g}^{z\nu}$) and QSR ($T \propto h^{\frac{z\nu}{\beta+\gamma}}$), respectively. (c) The specific heat, which follows $C \propto T$ within the QSR, reveals the crossover line with a power-law scaling of $T \propto h^{\frac{z\nu}{\beta+\gamma}}$ (see inset). (d) The calculated spin-lattice relaxation rate $\mathcal{S}_1(\omega = 0)$, which exhibits a power-law scaling of $T^{(\eta+d-2)/z}$ within the QSR, whose peak locations also reveal the QSR crossover line (see inset).

networks, $1/T_1$ can be efficiently calculated via $\mathcal{S}_1(0) \simeq \beta \sum_{\alpha} \langle S_i^{\alpha} \langle \frac{\beta}{2} \rangle S_i^{\alpha} \rangle$ [63], with $\beta \equiv 1/T$. In Fig. 6(d), we uncover pronounced spin fluctuations within the QSR, characterized by a universally diverging $1/T_1 \propto T^{(\eta+d-2)/z} \propto T^{-3/4}$, with an anomalous dimension $\eta = 1/4$. Upon approaching the QSR crossovers, $\mathcal{S}_1(0)$ reaches a maximum and then becomes suppressed. From the behaviors of $\mathcal{S}_1(0)$, the QSR crossover line can also be determined as illustrated in the inset of Fig. 6(d).

To comprehend these quantum scaling laws, we note that near the QCP, the singular free energy density adheres to the hyperscaling ansatz

$$F^{(s)} = T^{\frac{d}{z}+1} \psi_F(h T^{-\frac{\beta+\gamma}{z\nu}}, \tilde{g} T^{-\frac{1}{z\nu}}), \quad (1)$$

where $\psi_F(x, y)$ is a universal hyperscaling function with $x \equiv h T^{-\frac{\beta+\gamma}{z\nu}}$ and $y \equiv \tilde{g} T^{-\frac{1}{z\nu}}$. The $\psi_F(x, y)$ is a parity-even function of x , determining the scaling behavior of the critical system. Consequently, the singular part of specific heat is expressed as $C^{(s)} = T^{\frac{d}{z}} \psi_C(x, y)$, with $\psi_C(x, y)$ also a parity-even function of x . The peak of C/T illustrated in Fig. 6(c) is also linked to the maximum of the hyperscaling function $\psi_C(x_0, 0)$, implying that $\frac{\partial \psi_C(x_0, 0)}{\partial x} = 0$. Then, the QSR crossover line is characterized by the scaling relation $x = x_0$, i.e., $h = x_0 T^{\frac{\beta+\gamma}{z\nu}}$. The crossover line of the QSR is markedly different from the QCR crossover $\tilde{g} = y_0 T^{\frac{1}{z\nu}}$. Beyond the hyperscaling function of free energy, we find that

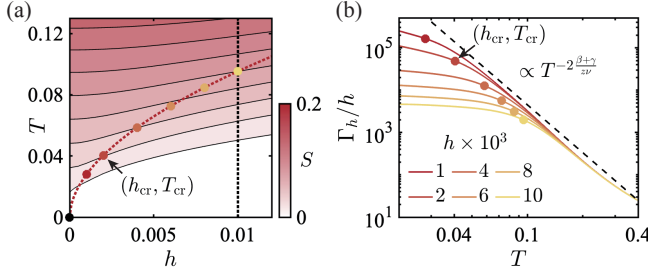


FIG. 7. (a) The isentropes in the h - T plane. The red dashed line represents the crossover line. (b) Results of Grüneisen ratio Γ_h with various fixed h . The black dashed line illustrates the quantum scaling $\Gamma_h/h \propto T^{-2\frac{\beta+\gamma}{z\nu}}$. The red circles ($h_{\text{cr}}, T_{\text{cr}}$) are determined from Fig. 2 of the main text and roughly mark the turning point where Γ_h deviates from the scaling law.

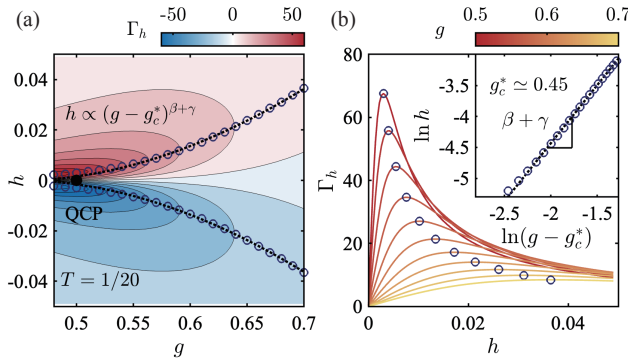


FIG. 8. (a) Contour of Grüneisen ratio Γ_h in the g - h plane at a fixed temperature $T = 1/20$. The blue hollow circles indicate the peaks/dips of Γ_h by scanning h for various fixed g . The curves of Γ_h vs. h are shown in (b). Inset illustrates the power-law scaling $h \propto (g - g_c^*)^{\beta+\gamma}$ of the peak locations, with our fit yielding $g_c^* \simeq 0.45$.

the spin dynamics at finite temperature also adheres to a universal hyperscaling form $S_1^{(s)} = T^{(d+\eta-2)/z} \phi_{S_1}(x, y)$. Consequently, the power-law scaling can also be observed in the relaxation rate behavior, as shown in Fig. 6(d).

Quantum supercritical scaling of Grüneisen ratio Γ_h .— Derived by free energy [Eq. (1)], the singular part of entropy also has a universal form

$$S^{(s)} = T^{\frac{d}{z}} \psi_S \left(h T^{-\frac{\beta+\gamma}{z\nu}}, \tilde{g} T^{-\frac{1}{z\nu}} \right) \quad (2)$$

near the QCP. In the QSR (with $\tilde{g} = 0$), the hyperscaling function becomes a one-variable function $\psi(x, y) \rightarrow \phi(x)$. Due to the symmetry with respect to the field h , $\phi_S(x)$ is a smooth and parity-even function which can be expanded as $\phi_S(x) = \sum_{i=0}^{\infty} A_{2i} x^{2i}$. Then, the singular part of Grüneisen ratio Γ_h can be expressed as

$$\Gamma_h^{(s)}(h, T) \Big|_{x \rightarrow 0} = \frac{\left(\frac{\partial S^{(s)}}{\partial h} \right)_T}{T \left(\frac{\partial S^{(s)}}{\partial T} \right)_h} \Big|_{x \rightarrow 0} \approx \frac{T^{\frac{d}{z} - \frac{\beta+\gamma}{z\nu}} 2A_2 x}{\left(\frac{d}{z} \right) T^{\frac{d}{z}} A_0}. \quad (3)$$

As we can see, Γ_h has a universal form $\Gamma_h^{(s)} = T^{-\frac{\beta+\gamma}{z\nu}} \phi_h(x)$, with $\phi_h(x) \propto x$ for small x [see Fig. 2(f) in the main text].

Therefore, when following the black dashed line with fixed h in Fig. 7(a), the Grüneisen ratio follows $\Gamma_h/h \propto T^{-2\frac{\beta+\gamma}{z\nu}}$ in the QSR, as shown in Fig. 7(b). This scaling law with $2(\beta+\gamma)$ boost is deviated until it approaches the QSR crossovers (solid circles in Fig. 7(a)).

Crossover scalings in the g - h plane.— Figure 8(a) shows the isothermal cut of Grüneisen ratio Γ_h at a fixed temperature $T = 1/20$. The Grüneisen ratio Γ_h exhibits peak/dip of h for each fixed $g \neq g_c$, as illustrated in Fig. 8(b). As shown in the inset, the peak locations follow $h \propto (g - g_c^*)^{\beta+\gamma}$, with g_c^* the pseudo-QCP estimated at finite temperature. In the zero-temperature limit, g_c^* approaches g_c and the crossover line follows $h \propto (g - g_c)^{\beta+\gamma}$.

To comprehend such crossover scalings, we consider the zero-temperature limit, $T \rightarrow 0$ ($x \gg 1, y \gg 1$), where the Grüneisen ratio follows $\Gamma \propto h^{-1} (\tilde{g}^{-1})$ scaling [11]. Thus, the hyperscaling function has the form

$$\psi_{\Gamma_h}(x, y)|_{x, y \rightarrow \infty} \approx B_1 x^{-1} + B_2 y^{-\beta-\gamma} + B_3 x^a y^b, \quad (4)$$

where $B_{1,2,3}$ are constant coefficients and a, b are undetermined parameters. In the zero-temperature limit, $\Gamma_h|_{T \rightarrow 0} = T^{-\frac{\beta+\gamma}{z\nu}} \psi_{\Gamma_h}(x, y)|_{x, y \rightarrow \infty} \rightarrow \text{const.}$, the B_3 term gives rise to a constraint $(\beta + \gamma)(a + 1) + b = 0$ between the exponents. Then, to locate the peak/dip in Fig. 8(b), we require $\frac{\partial \psi_{\Gamma_h}(x, y)}{\partial y} = 0$. Therefore, we take derivative of Eq. (4) vs. y , use the above exponent constraint, and obtain $x \propto y^{\beta+\gamma}$, i.e., $h \propto \tilde{g}^{\beta+\gamma}$.

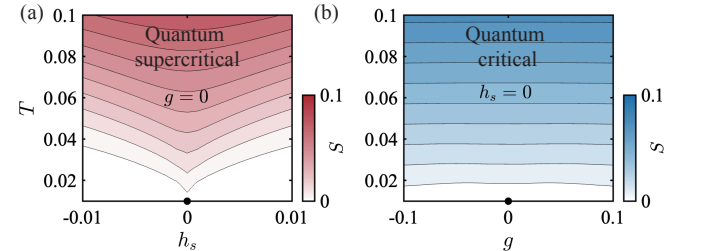


FIG. 9. Isentropic lines of (a) quantum supercritical cooling driven by staggered field h_s and (b) quantum critical cooling driven by uniform field g . We observe that the former significantly surpasses the latter in temperature variations.

Quantum critical versus supercritical cooling in the easy-plane XXZ chain.— The HDM chain under an external field can be transformed into an easy-plane XXZ chain, with both in-plane uniform field g and staggered field h_s . The field g induces a BKT-type quantum phase transition near the zero-field QCP, while h_s couples to the order parameter, giving rise to quantum supercriticality. In Fig. 9, we show the calculated isentropes of easy-plane Heisenberg chain ($\Delta = 0.5$) under field h_s [panel (a)] and g [panel (b)]. From the results, we find that the field h_s can drive a much more dramatic temperature variation as compared to the quantum critical cooling induced by the field g .